JOURNAL OF GEOPHYSICAL RESEARCH, VOL. 114, A02219, doi:10.1029/2008JA013080, 2009

FAST observations of downward current regions: Effect of ionospheric constraints on parallel signatures

K.-J. Hwang,[1] K. A. Lynch,[2] D. L. Newman,[3] and C. W. Carlson[4]

Received 6 February 2008; revised 31 October 2008; accepted 12 December 2008; published 21 February 2009.

[1] Downward current region auroral crossings by the FAST (Fast Auroral Snapshot) spacecraft show that divergent electric fields which are perpendicular to the geomagnetic field ($\mathbf{E}_\perp$) have two types of structures: those whose potential contours close below the spacecraft but above the ionosphere (U-shaped), and those that are not completely closed but partially couple to the low-altitude ionosphere (composite). Using FAST data from above 3000 km altitude, we investigate parallel signatures of particle motions in these downward current regions, focusing on the distinctions between U-shaped and composite potential structures. We analyze probability density functions of electron velocity moments and ion energies, and power spectral density scaling laws of wave turbulence above the potential drop. Results indicate that U-shaped potential structures show aspects of fully developed turbulence. Composite structures are often characterized by intermittent signatures, possibly because of lower ionospheric constraints. These results support a picture of an evolutionary process from composite to U-shaped potential structures in downward current regions.

Citation: Hwang, K.-J., K. A. Lynch, D. L. Newman, and C. W. Carlson (2009), FAST observations of downward current regions: Effect of ionospheric constraints on parallel signatures, *J. Geophys. Res.*, *114*, A02219, doi:10.1029/2008JA013080.

1. Introduction

[2] An investigation of intense, diverging DC electric fields perpendicular to the ambient magnetic field ($\mathbf{E}_\perp$) at Freja altitudes (1400 km) formed the basis for the prediction of sheetlike positive-potential structures in downward current regions (DCR). These potential structures are the counterpart to the negative-potential structures of visible aurora [*Marklund et al.*, 1997]. The FAST satellite provided conclusive evidence to confirm this positive-potential structure. However, a significant fraction of FAST DCR data was found to need more complicated, higher-dimension geometries than simple sheets. *Hwang et al.* [2006a, 2006b] show from $\mathbf{E}_\perp$ analysis that these DCR potential structures have varied and interesting structure both perpendicular and parallel to the geomagnetic field, with implications for models of their evolution and their coupling to the ionosphere.

[3] Statistical analysis of FAST $\mathbf{E}_\perp$ observations in auroral downward current regions shows several differences between sheetlike $\mathbf{E}_\perp$ field events, where the ratio of the two $\mathbf{E}_\perp$ components remains constant during the spacecraft crossing, and curved structures where the ratio varies. Sheetlike structures can be interpreted as straight arcs, but curved structures require gradients in another dimension. An important finding is that a significant fraction (more than half) show $\mathbf{E}_\perp$ signatures indicative of curved potential structures rather than idealized straight arcs [*Hwang et al.*, 2006a].

[4] Separately, a parameter η is defined as a proxy for the ratio of the potential, obtained by integrating $\mathbf{E}_\perp$ at the spacecraft, to the upgoing electron characteristic energy, defined as the energy flux divided by the number flux. Note that η should be close to 1 if the potential contours are completely closed below the spacecraft, i.e., U-shaped potential structures. η is thus a measure of the extent to which the potential contours are closed below the spacecraft. Statistical comparison shows that U-shaped closed-potential models are mostly consistent with curved events and that ionospheric effects where η is significantly less than 1 are dominant in sheetlike structures [*Hwang et al.*, 2006b]. Table 1 summarizes the number of events used in this paper classified by the two categories: U-shaped or composite, and curved or sheetlike. (Note that 7 events among the 71 examples used by *Hwang et al.* [2006a, 2006b] are discarded due to unavailability of high time resolution particle burst data required for the study presented in this paper). Changing event refers to an event that varies its $\mathbf{E}_\perp$ morphology between curved and sheetlike structures during the spacecraft crossing [*Hwang et al.*, 2006a]. Consistencies between U-shaped and curved events,

[1]NASA Goddard Space Flight Center, Greenbelt, Maryland, USA.
[2]Department of Physics and Astronomy, Dartmouth College, Hanover, New Hampshire, USA.
[3]Center for Integrated Plasma Studies, University of Colorado, Boulder, Colorado, USA.
[4]Space Sciences Laboratory, University of California, Berkeley, California, USA.

0148-0227/09/2008JA013080$09.00

Table 1. A Summary of the Number of Events Classified by Two Categories[a]

	U-Shaped	Composite
Curved	28	3
Sheetlike	2	26
Changing	4	1

[a]U-shaped or composite, and curved or sheetlike [*Hwang et al.*, 2006b]. Changing event is referred to as an event that varies its $\mathbf{E}_\perp$ morphology between curved and sheetlike structures during the spacecraft crossing [*Hwang et al.*, 2006a].

and between composite and sheetlike events are strong. This result implies that the spatial structure of the events, as indicated by the ratio of the $\mathbf{E}_\perp$ components, allows us to distinguish ionospheric fields and U-shaped potentials.

[5] These properties can be interpreted in the context of different potential closure models for sheetlike and curved structures, with important implications for models of the formation and evolution of potential structures for downward current regions. One possible evolutionary scenario is proposed on the basis of earlier numerical studies about the coupling between the low-altitude charge-depleted ionosphere and the high-altitude magnetosphere [*Streltsov and Lotko*, 2003]. In this model, an externally imposed downward current which evacuates the lower ionosphere gives rise to a conductivity hole in the lower ionosphere. This requires an enhanced $\mathbf{E}_\perp$ which couples along the field lines to the magnetosphere. Ions are pushed away horizontally from the center of the downward current sheet, and electrons are accordingly moved along the magnetic field away from the region. As a result, the field line becomes charge-carrier limited, and U-shaped potentials can form on the flux tubes defined by these ionospheric potential gradients (see Figure 1).

[6] According to the proposed evolutionary scenario, during the earliest stages of the formation of the U-shaped potential structures from within the ionospherically defined structures, the nested U-shaped potentials are not free enough to form folds or filaments according to Kelvin-Helmholtz instabilities. At a later time, after the relaxation of the ionospheric field and widening of the current channel [*Marklund et al.*, 2001], the high-altitude potential can form folds or filaments which are observed as curved structures by FAST.

[7] These studies show that auroral downward current regions have complex potential structures which, unlike upward current regions, are closely tied to the ionospheric responses. Based on these previous studies, in this paper, we examine these environmental effects of the ionospheric constraint by focusing on the differing parallel signatures of particle motions in the U-shaped (curved) and composite (sheetlike) structures. In this present paper, we assume the result of *Hwang et al.* [2006b], that is, that curved structures represent U-shaped potentials, and that sheetlike structures are composite. We refer to the U-shaped and composite classification rather than the more morphological sheetlike/curved one, as it represents a more fundamental view of the auroral processes we are studying.

[8] This work builds on FAST observations [*Ergun*, 2003; *Andersson*, 2002] and 1-D numerical studies of $\mathbf{E}_\parallel$ and electrostatic turbulence above the DCR potential drop [*Newman et al.*, 2001]. Direct observations of $\mathbf{E}_\parallel$ and

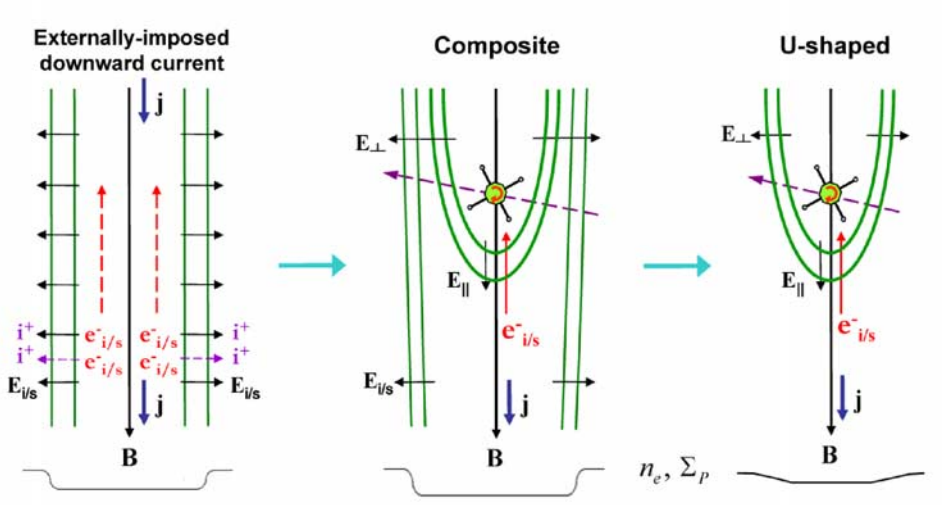

Figure 1. An evolutionary scenario for the DCR potential structure (left) from ionospheric fields only, (middle) through composite: ionospheric potential plus U-shaped potential, (right) to U-shaped structures [*Hwang et al.*, 2006b]. The index 'i/s' stands for ionosphere. Ionospheric equipotentials, which are initiated by the formation of ionospheric density depletion (illustrated at the bottom in black) at the footprint of the downward current channel and accelerate ionospheric ions (dotted violet arrows) away from the center of the current channel, are represented as thin green lines. U-shaped potentials, which can be formed according to the need for a supply of ionospheric current carriers, are represented as thick green lines. Representative FAST trajectories are shown as violet dashed arrows, and upgoing ionospheric electrons are shown as red arrows. The predicted evolution of ionospheric density or conductivity structures is illustrated at the bottom of each panel.

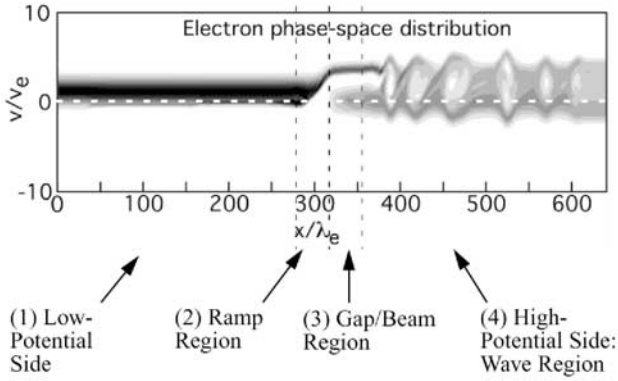

Figure 2. A snapshot of the evolved electron distribution from a 1-D Vlasov simulation of $\mathbf{E}_{\parallel}$ in the downward current region, from *Ergun* [2003], simulated by *Newman et al.* [2001].

electrostatic turbulence have been reported in the downward current region [*Ergun*, 2003; *Andersson*, 2002], showing measurements of parallel electric fields and electron fluxes, indicative of the localized parallel potential drop (double layer) that is responsible for particle acceleration [*Ergun*, 2003]. The Buneman-like convective instability is observed to grow away from the double layer, leading to strong wave turbulence roughly 10 Debye lengths above the double layer which quickly thermalizes upgoing electron beams [*Andersson*, 2002]. These observations are supported by numerical simulations. Figure 2 shows a 1-D Vlasov simulation [*Newman et al.*, 2001] of a double layer along a downward current region flux tube. The parallel structure includes: a low-potential region with low-frequency turbulence, a nearly monotonic potential ramp region with $\mathbf{E}_{\parallel}$, a beam region with an unstable electron beam at a similar characteristic energy to the potential of the ramp, and turbulent regions with intense electrostatic waves and nonlinear structures interpreted as electron phase-space holes.

[9] A turbulence analysis using FAST data is reported by *Chaston et al.* [2006] using interferometric techniques to study ionospheric density erosion by Alfvénic activity above the dayside auroral oval. In this study, the electric field power law spectra fits the Kolmogorov five-thirds law (for $k_{\perp}\lambda_e < 1$) on the assumption that wave frequency or the observed phase structuring is largely due to Doppler shift. Deviations from the Kolmogorov-like power law at wavenumbers a few times smaller than electron inertial length, $2\pi/\lambda_e$ are interpreted as wave dissipation through electron Landau damping when $k_{\perp}\lambda_e \rightarrow 1$.

[10] Unlike this Alfvénic turbulence study, most DCR turbulence has been studied more qualitatively. The broad-band wave power below 1 kHz, called BBELF (Broad-Band Electrostatic Low-Frequency) wave activity, almost always observed in the downward current region, has been modeled as electrostatic turbulence since there are no salient observations of the magnetic activity. This intense electrostatic turbulence is observed to rapidly stabilize the accelerated electron distributions and heat ions transversely forming ion conics [*Andersson*, 2002; *Lynch et al.*, 2002].

[11] These various turbulence properties can be quantified with FAST BBELF wave and particle measurements, and analyzed statistically in the context of turbulence theory for the two different types of DCR potential structures, U-shaped and composite. Moments of upgoing particle distributions are used as proxies for the potential drop behavior and implications for the ionospheric environment. Note that the temporal development of DCR structures takes a few hundred seconds according to Cluster observations [*Marklund et al.*, 2001]. These timescales are much larger than the timescales of the spacecraft crossing, so FAST can be assumed to observe snapshots of each stage of the evolution of the DCR turbulent region.

[12] The purpose of this paper is to determine from these turbulence analyses how parallel signatures of U-shaped and composite events differ, if the differences support the proposed evolutionary scenario in *Hwang et al.* [2006a, 2006b], and what role ionospheric boundary conditions play in parallel DCR signatures. In the following sections, we present statistical analyses of the velocity moments of ionospheric populations (section 2), and interpret the results based on turbulence theory (section 3). In section 4, we analyze the statistical power law invariant using BBELF wave data for the U-shaped and composite structures. Discussion and summary follow in sections 5 and 6.

[13] The statistical analysis made in this paper is based on 64 DCR events where strong (>100 mV/m) $\mathbf{E}_{\perp}$ events occur, taken from 50 FAST orbits at altitudes from 2500 km to 4100 km. The events are from either the prenoon dayside or near-midnight local time regions, and the data are comprised of FAST wave electric field measurements and high time resolution (sampling rate of 16 msec) particle burst data.

[14] Figure 3 shows an example from our FAST data sets. The panels show upgoing electron spectrogram covering 160°–200° pitch angles (Figure 3a), downgoing electron spectrogram covering 340°–20° pitch angles (Figure 3b), electron pitch angle distribution (Figure 3c), ion energy spectrogram covering all pitch angles (Figure 3d), ion pitch angle distribution (Figure 3e), the magnetic field fluctuation mostly in a longitudinal direction (Figure 3f), $\mathbf{E}_{\perp}$ data, with the geographic east-west component of $\mathbf{E}_{\perp}$ shown in black (east as positive), the north-south component in red (north as positive) (Figure 3g), and BBELF wave electric field spectrogram (Figure 3h). The positive slope in Figure 3f indicates that FAST crosses a downward current region during the most energetic upgoing electron event near 3 February 1997/19:29:16–20 UT. Electrons are predominantly upgoing aligned antiparallel to the direction of the geomagnetic field (Figure 3c), and ions maintain a conic distribution throughout the time series (Figure 3e), but intense conics are observed coincident with strong $\mathbf{E}_{\perp}$ (Figure 3g) and upgoing electron beams (Figure 3a). We calculate velocity moments and characteristic energies of electrons and ions near the center of a downward current sheet which can be determined from the $\mathbf{E}_{\perp}$ and particle signatures. The FAST crossing over the most intense event near the center of the current sheet corresponds to 3 February 1997/19:29:19 UT in this

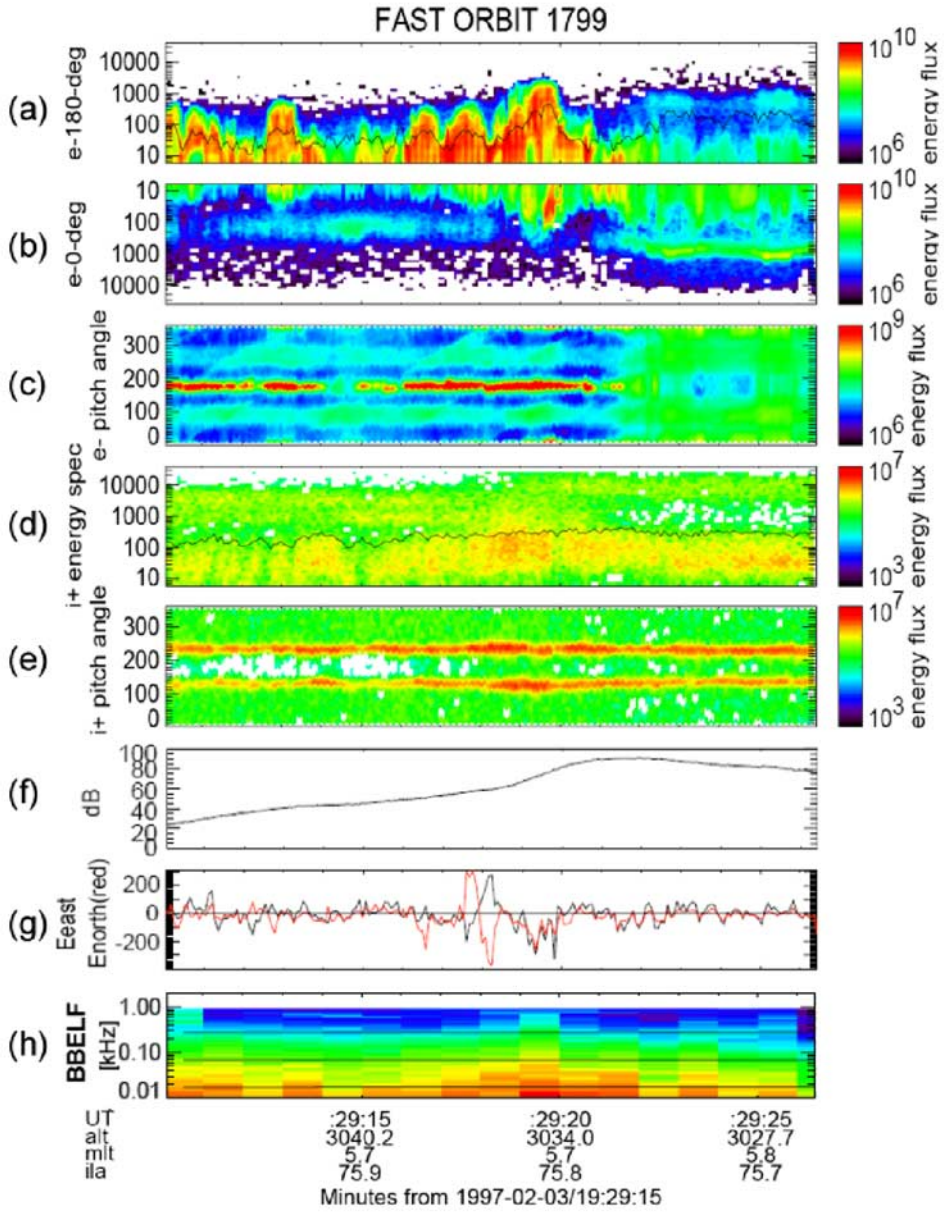

Figure 3. A FAST DCR crossing: (a) upgoing electron spectrogram, (b) downgoing electron spectrogram, (c) electron pitch angle distribution, (d) ion energy spectrogram of all pitch angles (thin black line represents ion characteristic energy defined as the energy flux divided by the number flux), (e) ion pitch angle distribution, (f) the magnetic field fluctuation, (g) two $\mathbf{E}_\perp$ components, east-west component of $\mathbf{E}_\perp$ shown in black, north-south component in red, and (h) BBELF wave electric field spectrogram.

example. Simultaneously, enhanced BBELF activity is observed in Figure 3h.

2. Analysis of Ionospheric Particle Velocity Moments

[15] Parallel electron motion above DCR potential drops is determined by both the magnitude of the potential drop and its variability, and by wave activity. The most common wave feature observed in the auroral downward current region is broadband electrostatic waves below 1 kHz (BBELF). The BBELF wave activity above the positive potential drop can thermalize energetic upgoing electron beams (and give further perpendicular heating to ion conics) while BBELF wave activity below the potential drop heats the ions perpendicular to the magnetic field, producing ion conics (upgoing ions of a conical velocity-space distribution centered on the magnetic field direction). Ion conic energies are also controlled by the magnitude of the potential drop through the pressure-cooker processes [*Gorney et al.*, 1985; *Lynch et al.*, 2002], where downpointing (earthward) DCR parallel electric fields retard the upgoing ion outflow until

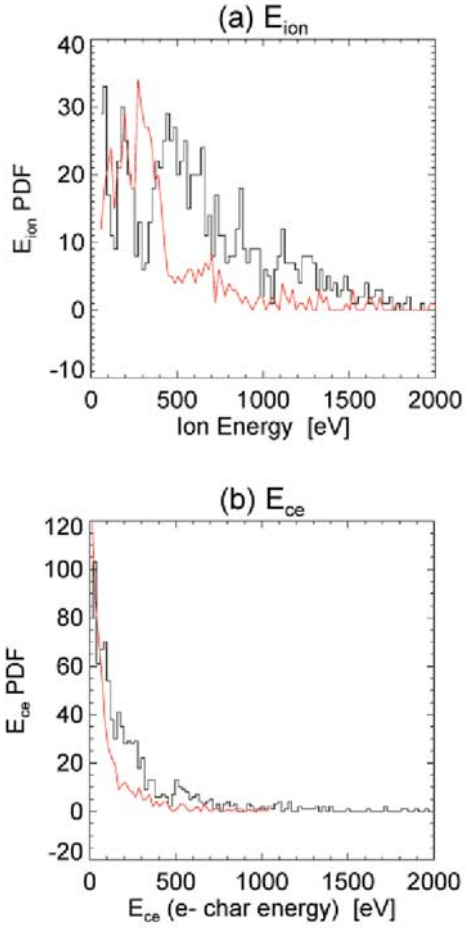

Figure 4. (a) Histograms of ion energies [eV], comprising ion drift energy along the magnetic field plus ion perpendicular thermal energies for the two types of different events. (b) Histograms of electron characteristic energy. Black (red) line corresponds to U-shaped (composite) potential events.

the ions acquire sufficient perpendicular energy by wave heating to overcome the $\mathbf{E}_{\|}$ with the magnetic mirror force conserving the first adiabatic invariant. Although heavier ions have a much longer response time to the variation of the potential drop than electrons do, their energy can reflect the degree of wave activity below and above the potential drop with implications for the potential drop magnitude. Thus both ion and electron moments provide information about the potential drop.

2.1. Ionospheric Energy Moments

[16] Figure 4a shows statistical histograms (probability density functions, or PDF), split into U-shaped and composite potential structure sets, for ion energies (in eV). These energies comprise ion drift energy along **B** plus ion perpendicular thermal energies, and use all the time series data in our statistics. The black line represents data from U-shaped potential events and the red, from composite events. T (or T mean) tests show that the two data sets are significantly different. U-shaped events peak at a higher ion energy (about 450 eV) than composite events (250 eV). Note that the low-energy peaks shown below 200 eV in the U-shaped events may indicate low-energy field-aligned ions of an extended (bimodal) conic distribution; these have been suggested to be caused by perpendicular energization which is extended along the field line, or by parallel acceleration processes as well as perpendicular acceleration [*Klumpar et al.*, 1984; *Temerin*, 1986; *Chang et al.*, 1986; *Peterson et al.*, 1992; *Miyake et al.*, 1996]. The higher-energy peak mainly comprises standard conic components. The mean ion energy for U-shaped events is 662 eV, and for composite events, 440 eV. This comparison implies that for U-shaped events the ions encounter a higher wave heating or stay a longer time within the heating region. Especially in the DCR high-potential side, wave turbulence is mainly generated by the accelerated, upgoing, electron beams [*Andersson*, 2002]. Therefore, a higher-magnitude potential drop will give rise to a stronger wave turbulence via more intense upgoing electron beams; also it can constrain pressure-cooker ions below the potential drop longer, which would be the case for the U-shaped events.

[17] PDF analyses of electron characteristic energies ($\boldsymbol{\epsilon}_{\mathbf{ce}}$) for the two types of events (Figure 4b) both show monotonically decreasing functions, but with different average $\boldsymbol{\epsilon}_{\mathbf{ce}}$ (264 eV for U-shaped, 128 eV for composite, significance = 5.5×10^{-19}). Sorting by $\boldsymbol{\epsilon}_{\mathbf{ce}}$ cannot clearly distinguish between U-shaped and composite events as discussed in Figure 4a. However, this $\boldsymbol{\epsilon}_{\mathbf{ce}}$ histogram is consistent with a higher potential drop magnitude, and therefore, a higher wave turbulence generated by the potential drop or a longer exposure time for ions to the heating, for the U-shaped events.

2.2. Ionospheric Electron Velocity Moments

[18] Figure 5 shows a scatterplot of the thermal velocity of field-aligned electrons versus the bulk velocity of the electron beams (Figure 5a), and the ratio of electron bulk velocity to its thermal velocity versus the bulk velocity (Figure 5b). Electron bulk flow or drift velocity along the magnetic field is obtained from the first moment calculation of electrons near the field line (340°–20° and 160°–200° pitch angles) and within an energy range of [6 eV, 40 keV], while the thermal velocity is from the second moment calculation (same energy and pitch angle ranges):

$$v_{\|} = \frac{1}{n}\int f_e(\mathbf{v}) v dv^3$$

$$v_{th} = \sqrt{\frac{1}{n}\int f_e(\mathbf{v})(v - v_{\|})^2 dv^3}$$

where $n = \int f_e(\mathbf{v}) dv^3$, the electron density calculated over the same pitch angle range as those for $v_{\|}$ and v_{th}. In this study both parallel and antiparallel ranges of electron pitch angle are chosen so that parallel motions of both antiearthward and earthward directions can be taken into account. Negative velocity here means the antiparallel direction, i.e., the upgoing antiearthward component in the northern hemisphere.

[19] Uncertainties in our data (shown in Figure 5, and hereafter) are calculated from those of the geometric factors of the electron and ion analyzer, which are found to vary <20% [*McFadden et al.*, 1999]. Other sources of data

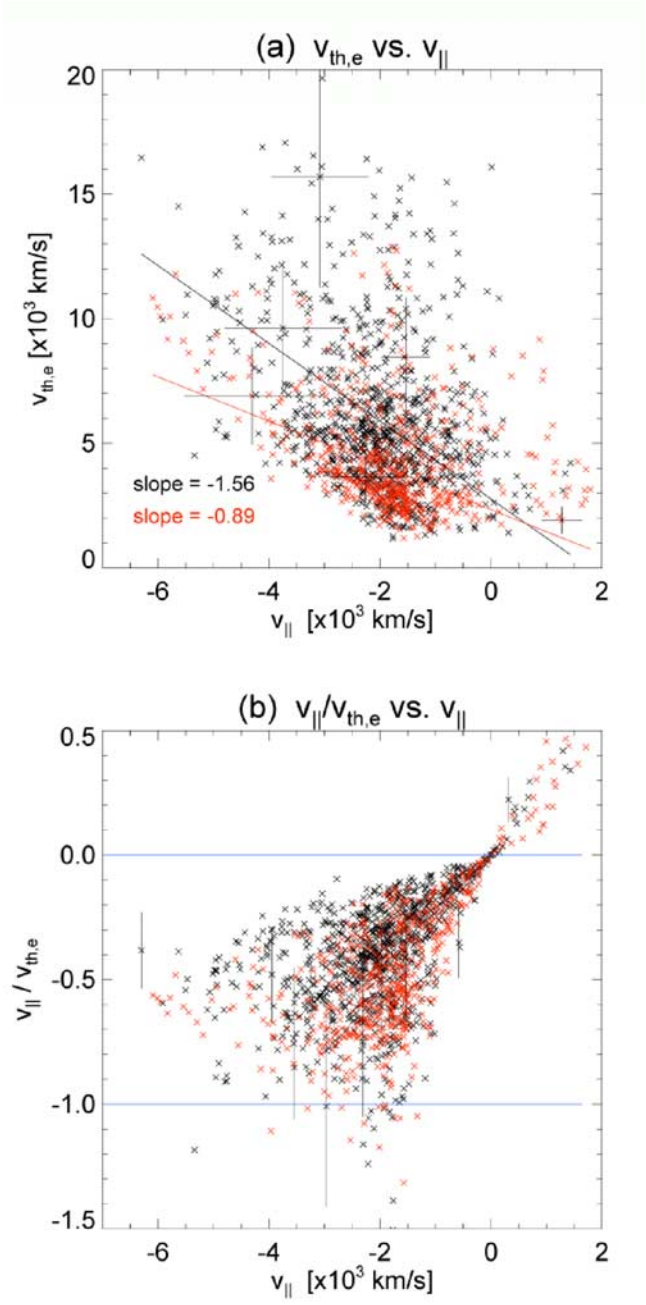

Figure 5. (a) A scatterplot of the thermal velocity of field-aligned electrons versus the bulk velocity of the electron beams, and (b) the ratio of electron bulk velocity to its thermal velocity versus the bulk velocity. In Figure 5a, black dots (from U-shaped events) are fit to a black line with a slope of −1.56, red dots (from composite events) to a red line of slope −0.89, showing that the upgoing electron beam is more strongly thermalized in U-shaped cases than in composite cases for a given $v_{||}$. Figure 5b shows that most of the data points reside within $|v_{||}/v_{th}| < 1$.

contamination are minor for the selected energy and pitch angle ranges for each of our data sets. The geometry-factor-derived uncertainties for a few representative points in each plot are marked as error bars.

[20] The electron drift velocity is a measure of the upgoing electron motion, which is related to the magnitude of the parallel potential drop, but degraded by wave-particle interactions with BBELF wave activity. It is noticeable that a small fraction of the data is shown to have net parallel drift velocities along **B** (downward). These earthward moving electrons might be caused by significant precipitating magnetospheric electrons, or by reflection of electrons back to the potential drop by the intense wave turbulence above the parallel potentials.

[21] In Figure 5a, black dots (from U-shaped events) are fitted to a black line with a slope of −1.56, and red dots (from composite events) to a red line of slope −0.89. (Again, the two data sets show a significant difference with significance of 2.5×10^{-5}.) This slope indicates how strongly the upward electron beam is thermalized for a given $v_{||}$. Thus, this plot shows that the upgoing electron beam is more strongly thermalized in U-shaped cases than in composite cases, indicating more intense turbulence in U-shaped cases. An interesting finding is found in Figure 5b where most of the data points reside within $|v_{||}/v_{th}| < 1$. Thermalization increases with $-v_{||}$, limiting $|v_{||}/v_{th}| < 1$.

[22] Figure 6a shows the PDF of electron drift velocity for composite (left) and U-shaped (right) events with red lines showing fits of these distributions to Gaussians, $f = C_1 e^{-C_2}(v_{||}-C_3)^2$, where three degrees of freedom, C_1, C_2, and C_3 are determined under the least squares method. The reduced chi-squared value, X, defined as

$$X^2 = \frac{s^2}{\sigma^2} = \frac{1}{N-p-1}\sum_{i=1}^{N}\left(\frac{y_i - f(x_i)}{\sigma_i}\right)^2 \qquad (1)$$

where N is number of data points, p is the degrees of freedom (number of fitting parameters), y_i is measured data, σ^2 is the variance of the measured y_i, $f(x_i)$ is the estimated fit, and s^2 is the estimated variance of the fit, is shown in each panel, showing a goodness of fit (for a better fit, X is closer to 1). Again, negative drift velocity corresponds to the direction antiparallel to the geomagnetic field.

[23] U-shaped events show a more Gaussian-like distribution than do composite events. (Not shown here, sorting by the sheetlike versus curved classification shows very similar patterns.) Note that the peak (most common) magnitude of the electron parallel drift velocity of 2000 km/s upward (antiearthward) for U-shaped events is a bit larger than the 1,700 km/s of the composite events.

[24] Figure 6b shows the PDF of electron thermal velocity for composite (left) and U-shaped (right) events with red lines fitted as Gaussians. Though both events show significant fractions of the distributions in their tails (at velocities about 7000 km/s for composite, at about 10,000 km/s for U-shaped), the U-shaped event distribution is more Gaussian than the composite according to the comparison of X values. Again note that the peak magnitude of electron thermal velocity at around 4800 km/s for U-shaped events is greater than the 3,300 km/s of the composite events. The difference in thermalization of electrons is more distinct than is that of the upflowing electron drift velocity.

[25] Figure 6c shows the PDF of the ratio of electron drift velocity to the thermal velocity for composite (left) and U-shaped (right) events with red lines fitted as Gaussians.

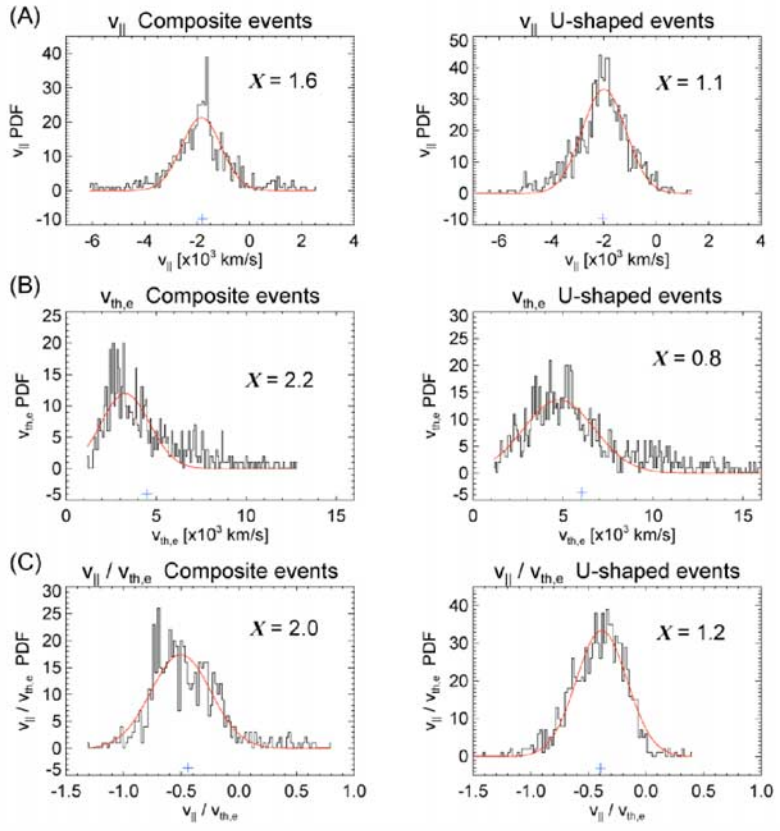

Figure 6. Probability density functions (PDF) of (a) electron drift velocity for (left) composite and (right) U-shaped events with red lines fitted as Gaussian; (b) electron thermal velocity for (left) composite and (right) U-shaped events; (c) the ratio of electron drift velocity to the thermal velocity for (left) composite and (right) U-shaped events. The reduced chi-squared value X (for a better fitting, X is closer to 1) for a Gaussian fit (red curve) is shown in each panel. A blue mark near the bottom of each panel indicates a mean value of each parameter.

Again the U-shaped distribution is more Gaussian than is the composite. The Gaussian peak of $|v_{||}/v_{th}|$ for composite is 0.48, which is greater than U-shaped $|v_{||}/v_{th}|$ peak of 0.41.

[26] Blue marks near the bottom of each panel show the mean value, which is coincident with the peak of the Gaussian fit for the cases of a good fitting with a relatively symmetric distribution around its peak value. The mean value is not coincident with the Gaussian peak when the measured PDF is asymmetric, even though the reduced chi-squared value is close to 1, as shown in Figure 6b.

3. Interpretation: Electron Parallel Velocity Moments and Gaussian Distributions

[27] These statistical studies of electron velocity moments and ratios are carried out with only relatively field-aligned electrons taken into account, simplifying the analysis to one dimension in the gyrotropic environment near the center of the DCR current sheet. This also prohibits the inclusion of other factors beyond the effect of electrostatic turbulence on particles' parallel motions, such as boundary effects near the U-shaped potential contours. The results are as follows. For all electron velocity moments, $v_{||}$ obtained from the first moment of electrons, $v_{||,\varepsilon_{ce}}$ from electron characteristic energy ε_{ce} (not shown), and v_{th} from the second moment, we find that U-shaped events have greater peak values in PDF distributions. The difference in v_{th} between U-shaped and composite events is more significant than the difference in $v_{||}$, resulting in a smaller $v_{||}/v_{th}$ ratio for U-shaped than for composite events. In addition, the shapes of the histograms of electron velocity moments ($v_{||}$, v_{th}, and their ratio $v_{||}/v_{th}$) show that U-shaped events are more Gaussian than composite events.

[28] In general, when applying PDF analysis to classical turbulence theory, it should be noted that turbulence or intermittency theory refers to turbulent situations characterized by a high degree of symmetry, requiring spatial homogeneity with rotational isotropy [*Batchelor*, 1953; *Frisch*, 1995]. Spatial homogeneity means that the statistical properties of turbulence do not change under spatial translations. Quantitatively, within the volume of interest, these statistical properties should not change over dimensions that are large compared to the wavelengths of the turbulence, in the Fourier-space decomposition of the field, whatever the field may be (velocity, electric field, mass density, etc.). Rotational isotropy means that the statistical properties of the turbulent field are invariant under spatial rotations about any axis [*Batchelor*, 1953; *Frisch*, 1995].

Thus, in our case, where there is present a strong DC magnetic field, there is a good likelihood that plasma turbulence will not be isotropic, and this symmetry will be broken. It is important to check if the auroral plasma we are studying is homogeneous or isotropic enough to have confidence in theories that start by assuming homogeneity and isotropy. In fact, there is generally little chance to satisfy such symmetries in that the high potential side of the downward current region is neither huge in space nor far away from its generation location.

[29] Here we have focused on one-dimensional parallel motion of accelerated plasma which is predominantly thrown by the parallel potential onto the background of isotropic magnetospheric plasmas on the high-potential side of the downward current region below the FAST observation point. This situation is similar to wind tunnel experiments producing eddy motion at all scales, suggesting that some form of statistically homogeneous turbulence may be present [*Frisch*, 1995]. During the very short time (1–3 s) of FAST crossing near the center of a downward current sheet (in order to avoid the boundary effects), we can assume that the FAST spacecraft is almost stationary compared to the upward electron flows in such a way that the observed structure can be treated as predominantly temporal. Limiting our study to a one-dimensional analysis also conciliates the anxiety about the isotropy requirement under the strong background magnetic field.

[30] For a test of how much the other requisite symmetry, i.e., the homogeneity of the plasma through which FAST is flying, can be assumed, we made histograms of the measured parameters (electric fields and velocity fields) as the spacecraft flies through the turbulent regions at different altitudes in different events, to see how the shape of the probability distribution functions varies from event to event. The PDFs obtained from different FAST crossings at different altitudes are qualitatively the same.

[31] In turbulence theory of homogeneous fluids, purely turbulent fluids or fully developed stages of turbulence always show Gaussian (normal) distributions of all relevant parameters. In contrast, deviations from Gaussians can be interpreted as intermittency [*Batchelor*, 1953; *Frisch*, 1995]. In the auroral downward current region environment, the accelerated electron beams immediately above the parallel potential drop are highly collimated with a relatively narrow parallel velocity distribution around the velocity corresponding to the magnitude of the potential drop. The only cause for these narrow electron beams to be distributed more randomly in the parallel velocity space is a strong BBELF wave turbulence, which produces a qualitatively similar distribution among different FAST orbits as tested. This is why turbulence theory can reasonably be applicable to our interpretations of the measured velocity moment PDF analyses, beyond interpretations from the point of view of the central limit theorem. The measured velocity moments in Figure 6 are influenced by many small interactions with wave turbulent forces. In the case of U-shaped events, a sufficient number of such small interactions may lead to a Gaussian distribution of their velocity moments, possibly giving rise to the fully developed turbulent state. In less developed turbulences for composite events, there may be an insufficient number of small scatterings which leads to not fully developed turbulence, or intermittent state. Note that it is shown in section 2 that there is a salient evidence of a weaker turbulence for composite events than for U-shaped ones.

[32] Note that one assumption underlying the central limit theorem is that all of the cumulative measurements are statistically independent of one another. For instance, if two measurements are too close together in time, they may be mutually correlated, even in the fully turbulent regime. If such measurement-based correlations contribute to non-Gaussian behavior for the composite events, then it should similarly contribute for the U-shaped events, since the measurement rate is the same in both events. This is not the case for our PDF results. Therefore, based on the PDF analyses in the previous section, we demonstrate that U-shaped events can be interpreted as showing fully developed turbulence, while composite events demonstrate not fully developed turbulence or intermittency.

4. Interpretation: BBELF PSD Analysis

[33] In this section, we investigate wave power spectral density (PSD) distribution to support our conclusions derived from the PDF analyses of electron velocity moments in sections 2 and 3. Figure 3 illustrates a typical auroral downward current region signature, where BBELF wave turbulence of frequencies below 1 kHz are observed to be enhanced during the event (Figure 3h). We analyze the statistical power law scaling factor using these BBELF wave electric field data for each of both U-shaped and composite events.

[34] Figure 7a shows the PSD of the broadband wave turbulence shown in Figure 3h between 3 February 1997/ 19:29:19–20 UT. During this time, FAST was crossing a composite potential structure, observing a sheetlike morphology as shown in Figure 3g. A fitted spectral slope is about −3.01. A comparative U-shaped example is shown in Figure 7b, where the fitted spectral slope of −1.66 corresponds to the Kolmogorov five-thirds law ($dW/df \approx f^{-5/3}$, where W is wave power, and f is frequency) in turbulence theory.

[35] A statistical result of the power law scaling factor for U-shaped and composite events is shown in Figure 7c. For our statistics, we excluded the events where the correlation coefficient between measured PSD data and the fitted line is less than 0.9. Black stars represent U-shaped events, and red ones composite events. The x axis numbers each data set, and the y axis shows a PSD power law scaling factor; the scaling invariant according to Kolmogorov five-thirds law is indicated by a black horizontal line. Clearly, a majority of U-shaped events is located close to the Kolmogorov five-thirds line, while composite events are broadly distributed from −3.5 to −1.

[36] This strongly suggests that during the time of the FAST crossing of U-shaped structures, it would more probably encounter fully developed states of wave turbulence than intermittent states. These might, in turn, give rise to Gaussian-like velocity moment distributions to the upgoing field-aligned electrons passing through the wave heating region. On the contrary, when FAST crosses a composite structure, it would be likely to observe intermittent signatures of wave turbulence, which might, in turn,

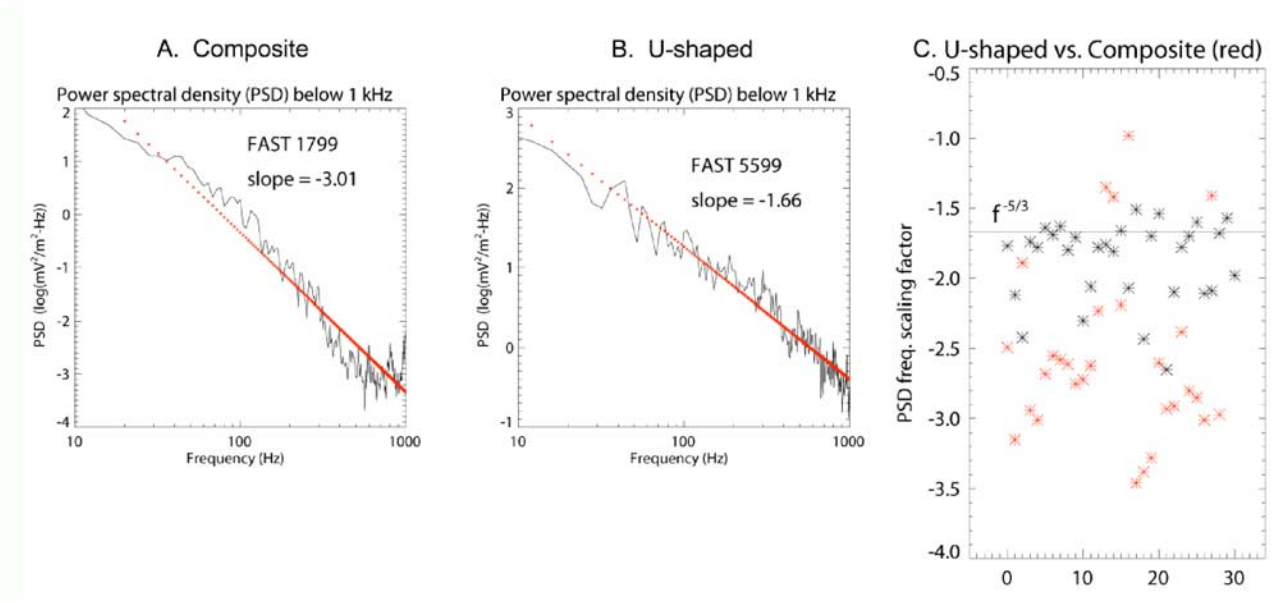

Figure 7. Power spectral density (PSD) plots of the broadband wave turbulence. (a) A composite example, shown in Figure 3h between 3 February 1997/19:29:19–20 UT. (b) A U-shaped example, where the fitted slope of −1.66 corresponds to the Kolmogorov five-thirds law ($dW/df \approx f^{-5/3}$, where W is wave power, and f is frequency). (c) A statistical result of the power law scaling factor for U-shaped events (black) and composite ones (red).

produce a significant deviation from Gaussian distribution of the electron velocity PDFs.

5. Discussion

[37] Motivated by turbulence theory, PDF analysis of electron velocity moments is carried out to show that U-shaped events are likely to produce more Gaussian distributions, consistent with fully developed turbulence signatures above the $\mathbf{E}_{\parallel}$ region. In contrast, composite potential structures show deviations from Gaussian distributions, consistent with intermittent or not fully developed turbulent phenomena. A statistical analysis of the PSD scaling factor of BBELF waves for each event gives a consistent implication with the PDF analysis results.

[38] In the evolutionary scenario proposed, composite potentials correspond to the early stage of the formation of the potential drop with ionospheric constraints such as coupled ionospheric fields. At this stage these ionospheric constraints might prohibit the turbulent region above the potential drop from being fully developed. The structure itself is highly dependent on the lower ionosphere since the formation is triggered by lower ionospheric conductivity structures and this triggering would be inherently intermittent. U-shaped potentials correspond to the later stage in evolution, less constrained by the ionospheric constraints. The potential structure may then be in a relatively stable state after going through earlier, more variable, stages of the formation process. At this stage, the high potential side above the potential drop would provide an environment for fully developed turbulence, with velocity PDFs indicative of turbulent flow.

[39] Therefore, the intermittency observed in both the velocity PDF and the BBELF PSD is interpreted as the result of a close dependence on lower ionospheric constraints in the composite potential structures. This result supports our evolutionary path from composite structures to U-shaped, indicating that composite events are highly dependent on lower ionospheric constraints such as ionospheric field or conductivity structures.

[40] Another possible driver for the intermittent state of the DCR high-potential region might be the intermittent variability of high-altitude potential drop structures. This effect seems to be related to the background conditions of precipitating plasmasheet populations, which is discussed in the companion paper *Hwang et al.* [2009].

6. Conclusion and Future Work

[41] Following the two previous papers *Hwang et al.* [2006a, 2006b], we have investigated parallel particle signatures in downward current regions, focusing on the differences between U-shaped and composite potential structures. We demonstrate the following conclusions.

[42] 1. Ion populations above the potential drop, which have overcome the parallel potential drop via the ion pressure cooker, are more energetic in U-shaped cases than in composite. The higher ion energy for U-shaped events implies that the ions have experienced a higher ion-wave heating, or spent a longer time within the heating region.

[43] 2. Upgoing electron beams are more strongly thermalized in U-shaped cases than in composite, indicating that there exists a higher wave turbulence in the DCR high-potential side for U-shaped structures.

[44] 3. U-shaped or curved events show Gaussian distributions of the velocity moments above the potential drop. Also for U-shaped, the BBELF PSD scaling law tends to converge to the Kolmogorov five-thirds law. Both imply

that U-shaped potential structures might induce fully developed turbulence signatures above the $\mathbf{E}_{\parallel}$ region.

[45] 4. Composite structures show a significant deviation from Gaussian distributions, and their BBELF PSD scaling factors are not consistent with the Kolmogorov's turbulence regime. These might indicate that composite structures are often characterized by intermittent signatures, possibly due to their dependency on intermittent lower ionospheric conditions.

[46] These results support the proposed evolutionary process from composite to U-shaped potential structures, where composite potential events are constrained by low-altitude ionospheric parameters, while U-shaped structures tend to act independently of these constraints.

[47] The evolutionary scenario of the potential structure in the downward current region can be more firmly supported by a systematic understanding from the low ionosphere to an altitude of several R_E with help of ground-based optical data and by high altitude multisatellite data such as from CLUSTER. Another attempt is a numerical study, which is in progress, with a large simulation domain along the DCR flux tube in order that the feedback between the potential drop and both ionospheric and magnetospheric conditions can be investigated. These along-flux-tube conjunctive and computational studies will ultimately give a deeper understanding about ionosphere-magnetosphere coupling and DCR current-voltage relations. For this purpose, it is important to establish the effect of plasma sheet populations on the DCR potential drop behavior. In our companion paper, we examine these questions by focusing on the effect of magnetospheric boundary conditions.

[48] **Acknowledgments.** This work was supported by NASA grant NAG5-10472 and by Dartmouth College. We appreciate a helpful discussion with Christopher C. Chaston about our BBELF PSD results.

[49] Amitava Bhattacharjee thanks Michael Temerin and another reviewer for their assistance in evaluating this paper.

References

Andersson, L. (2002), Characteristics of parallel electric fields in the downward current region of the aurora, *Phys. Plasmas*, *9*, 3600.

Batchelor, G. K. (1953), The theory of homogeneous turbulence, in *Cambridge Monographs on Mechanics and Applied Mathematics*, Cambridge Univ. Press, New York.

Chang, T., G. B. Crew, N. Herkowitz, J. R. Jasperse, J. M. Retterer, and J. D. Winningham (1986), Transverse acceleration of oxygen ions by electromagnetic ion cyclotron resonance with broad band left-hand polarized waves, *Geophys. Res. Lett.*, *13*, 636.

Chaston, C., V. Genot, J. Bonnell, C. Carlson, J. McFadden, R. Ergun, R. Strangeway, E. Lunc, and K. Hwang (2006), Ionospheric erosion by Alfvén waves, *J. Geophys. Res.*, *111*, A03206, doi:10.1029/2005JA011367.

Ergun, R. (2003), Double layers in the downward current region of the aurora, *Nonlinear Processes Geophys.*, *10*, 45.

Frisch, U. (1995), *Turbulence*, Cambridge University Press, New York.

Gorney, D. J., Y. T. Chiu, and D. R. Croley (1985), Trapping of ion conics by downward parallel electric fields, *J. Geophys. Res.*, *90*, 4205.

Hwang, K.-J., K. Lynch, C. Carlson, J. Bonnell, and W. Peria (2006a), FAST observations of perpendicular DC electric field structures in downward auroral current regions: Morphology, *J. Geophys. Res.*, *111*, A09205, doi:10.1029/2005JA011471.

Hwang, K.-J., K. Lynch, C. Carlson, J. Bonnell, and W. Peria (2006b), FAST observations of perpendicular DC electric field structures in downward auroral current regions: Implication, *J. Geophys. Res.*, *111*, A09206, doi:10.1029/2005JA011472.

Hwang, K.-J., K. A. Lynch, D. L. Newman, and C. W. Carlson (2009), FAST observations of downward current regions: Effect of magnetospheric conditions on the parallel potential drop, *J. Geophys. Res.*, *114*, A02218, doi:10.1029/2008JA013079.

Klumpar, D. M., W. K. Peterson, and E. G. Shelley (1984), Direct evidence for two-stage (bimodal) acceleration of ionosphere, *J. Geophys. Res.*, *89*, 10,779.

Lynch, K. A., J. W. Bonnell, C. W. Carlson, and W. J. Peria (2002), Return current region aurora: $E_{\parallel}$, j_z, particle energization and BBELF wave activity, *J. Geophys. Res.*, *107*(A7), 1115, doi:10.1029/2001JA900134.

Marklund, G., T. Karlsson, and J. Clemmons (1997), On low altitude particle acceleration and intense electric fields and their relationship to black aurora, *J. Geophys. Res.*, *102*, 17,509.

Marklund, G. T., et al. (2001), Temporal evolution of acceleration structures in the auroral return current region, *Nature*, *414*, 724–727.

McFadden, J. P., C. Carlson, R. Ergun, D. Klumpar, and E. Moebius (1999), Ion and electron characteristics in auroral density cavities associated with ion beams: No evidence for cold ionospheric plasma, *J. Geophys. Res.*, *104*, 14,671.

Miyake, W., T. Mukai, and N. Kaka (1996), On the origins of the upward shift of elevated (bimodal) ion conics in velocity space, *J. Geophys. Res.*, *101*, 26,961.

Newman, D. L., M. V. Goldman, R. E. Ergun, and A. Mangeney (2001), Formation of doulbe layers and electron holes in a current-driven space plasma, *Phys. Rev. Lett.*, *87*, doi:10.1103/PhysRevLett.87.255,001.

Peterson, W. K., H. L. Collin, M. F. Doherty, and C. M. Bjorklund (1992), O^+ and he^+ restricted and extended (bi-modal) ion conic distributions, *Geophys. Res. Lett.*, *19*, 1439.

Streltsov, A. V., and W. Lotko (2003), Small-scale electric fields in downward current channels, *J. Geophys. Res.*, *108*(A7), 1289, doi:10.1029/2002JA009806.

Temerin, M. (1986), Evidence for a large bulk ion conic heating region, *Geophys. Res. Lett.*, *13*, 1059.

C. W. Carlson, Space Sciences Laboratory, University of California, Berkeley, CA 94720, USA. (cwc@ssl.berkeley.edu)

K.-J. Hwang, NASA Goddard Space Flight Center, Greenbelt, MD 20771, USA. (joohwang@umbc.edu)

K. A. Lynch, Department of Physics and Astronomy, Dartmouth College, Hanover, NH 03747, USA. (kristina.lynch@dartmouth.edu)

D. L. Newman, Center for Integrated Plasma Studies, University of Colorado, Boulder, CO 80309, USA. (david.newman@colorado.edu)